

# Influence of Strontium Addition on Microstructure and Mechanical Properties of an Al–10Si–5Cu Alloy

Hao Wan<sup>1</sup> · Naichao Si<sup>1</sup> · Guanglei Liu<sup>1</sup> · Chao Wei<sup>1</sup> · Bo Zheng<sup>1</sup> · Yushan Li<sup>1</sup>

Received: 11 September 2016 / Accepted: 7 December 2016 / Published online: 31 December 2016  
© The Indian Institute of Metals - IIM 2016

**Abstract** The microstructure and mechanical properties of Al–10Si–5Cu cast alloys with micro-addition of alloying elements (V, Cr and Ni) were studied before and after strontium addition. Samples were examined using the X-Ray diffraction, the optical microscope, the scanning electron microscope and the energy dispersive spectrometer. The results indicated that the  $\alpha$ -Al matrix, eutectic Si phase and Al<sub>2</sub>Cu phase were the main constituent phases of Al–10Si–5Cu alloys before or after strontium addition. Strontium addition affected the refining of the  $\alpha$ -Al grains and transforming the configuration of interdendritic phases. The un-modified alloy showed a brittle nature because of existing brittle and aggregated AlSiMnFe phases. Contributing to the alteration of microstructure in strontium modified alloy, the strength and elongation of the alloy were improved. In addition, the fracture mechanism and crack propagation process were investigated in both the alloys.

**Keywords** Aluminum alloy · Microstructure · Mechanical property · Fracture mechanism

## 1 Introduction

Al–Si–Cu based alloys constitute important aluminum alloys due to their low density, high specific strength, excellent cast-ability, mechanical properties and corrosion resistance [1, 2]. Hence, Al–Si–Cu based alloys have been widely used in automotive, mechanical industry and

aerospace [3–5]. Generally, the mechanical properties of cast Al–Si–Cu alloys mainly depend on the microstructure of the alloy, especially the size and morphology of  $\alpha$ -Al grains and the configuration of eutectic Si phase [6–8].

According to relevant work conducted by other authors, the performance of Al–Si–Cu alloys could be improved by adding alloying elements or reducing impurity elements in the melt [9–13]. Hekmat-Ardakan et al. [9] discovered that an increase in the content of Mg could transform coarse grained primary Si into fine grained Mg<sub>2</sub>Si. It was proved that fine grained Mg<sub>2</sub>Si had beneficial effects in improving the wear resistance of hypereutectic Al–Si–Cu alloy A390. Banerjee et al. [10] discovered that addition of Sn traces would increase the yield strength and ultimate tensile strength of Al–6.2Cu–0.6 Mg. Shaha et al. [11] added Ti, V and Zr traces, in a Al–7Si–1Cu–0.5 Mg alloy to form a plate-like Zr–Ti–V-rich phase and improve its' fatigue resistance. Moreover, Seifeddine et al. [12] discovered that the harmful effect of Fe could be relieved by adding Mn in the aluminum alloy. Yu et al. [13] discovered that the element Y had an affinity for H to form stable YH<sub>2</sub> and YH<sub>3</sub> hydride phases.

Alternatively, the mechanical properties of Al–Si–Cu alloys can be enhanced by grain refining or interdendritic phases modification. For achieving grain refinement, the most commonly used refiners are Al–Ti-based alloys [14, 15]. Furthermore, new refiners, such as Al–B, Al–Ti–B–RE and Al–Ti–B–C have been investigated [16–18]. In industrial applications, the elements Na, Sr and Sb have been extensively used in Al–Si alloys to modify the eutectic Si phase. However, the element Na does not have a sustainable phase modification effect [19]. Besides, Na increases the tendency of pore formation in alloy casting. In an alloy with Sb addition, the eutectic Si phase still exists in a lamellar configuration. Nevertheless, a small

✉ Naichao Si  
snc@ujs.edu.cn

<sup>1</sup> School of Materials Science and Engineering, Jiangsu University, Zhenjiang 212013, People's Republic of China

amount of strontium can transform the acicular lamellar eutectic Si phase to a fine fibrous phase configuration [20]. Actually, strontium participates in increasing twinning density when its' atoms are absorbed by the solid–liquid interface according to the twin plane re-entrant edge model [21]. Moreover, the growth of the eutectic Si phase can be restricted by a strontium aggregation. The RE elements (such as La, Eu, Yb, Y and Sc) have similar effects in modifying the eutectic Si phase with strontium, such as fine fibrous eutectic Si phase obtained in the Al–5Si alloy with an addition of 0.05 wt% Eu. The element Eu can restrain the growth of the eutectic Si phase by the formation Al<sub>2</sub>Si<sub>2</sub>Eu phases around it [22].

Recently, the use of a lighter aluminum engine has been proved to be the future in the automobile industry. An Al–7.5Si–4Cu alloy [3] (tensile strength, 233 MPa and elongation, 3.2%) in the fabrication of the cylindrical block and heads of the car engine has been applied. However, with the rapid development of automobile industry, the use of Al–Si based alloys with higher performance have become mandatory. Hence, based on the Al–7.5Si–4Cu alloy, it is believed that a new alloy with a higher strength and a good ductility can be produced. In this paper, the microstructure and the mechanical property of an Al–10Si–5Cu alloy with micro addition of alloying elements (V, Cr and Ni) have been studied before and after strontium addition. Moreover, the fracture mechanism and crack propagation behavior of experimental alloys have also been investigated.

## 2 Materials and Methods

Table 1 shows the chemical composition of the experimental alloy Al–10Si–5Cu. Ingots were melted in a 10 kg silicon carbide crucible in an electric resistance furnace at a temperature of 750 °C. The A356 ingots were melted as the base alloy. The alloying elements were melted in the form of master alloys of Al–30Si, Al–50Cu, Al–10Mn, Al–5Cr, Al–5Ni, Al–55 V, Al–5Zr and Al–10RE. Before the addition of commercially available pure Mg, Zn and Sn, the melt was cooled to 720 °C to decrease the burn loss of these low-melting point elements. In the alloy with microstructure modification, Al–10Sr master alloys were added. The degassing of the melt was executed by the argon furnace inlet (at a rate of 15 L/h) known as the

porous plug method. Then the melt was thermally held at 710 °C for 20 min to guarantee the homogeneity and the dissolution of the designed alloys. In the end, the melt was poured into a 30 × 120 × 220 mm sized stainless steel mold for solidification.

The as-cast samples were ground by a range of SiC sandpapers to 1000 grit. Following, the samples were polished with diamond spray polishing compounds to obtain a mirror surface effect. Then the mirror finished surfaces of the samples were etched by a Keller's reagent. An Optical microscope (OM) and a scanning electron microscope (SEM) were utilized to investigate the microstructure of the samples. Furthermore, certain special phases were studied by the electron energy disperse spectroscopy (EDS). In addition, for measuring the grain size in both as-cast and strontium modified Al–10Si–5Cu alloys, 20 OM images of the microstructure of both the alloys were processed and statistically analyzed by the Nano Measurer software.

For the assessment of micro-hardness alterations before and after strontium addition, the samples were tested on a HVS-1000 micro-hardness device. Fifteen uniformly distributed indentations were made with a Vickers pyramid indenter, and the distance between two indentations was set to greater than 100 μm. The indentation load of 300 N was applied and held for 10 s. For the tensile test, five specimens for each case, were prepared by a wire-electrode cutting according to Chinese standard GB/T 228.1-2010. The tensile properties tests were carried out by a computerized universal Instron 5581 tensile testing machine at room temperature. The speed of the crosshead was 1 mm/min. After the execution of the tensile test, the fracture surfaces and cross-sections of fractured specimen were observed by the SEM device for the morphology and mechanism of fracture study.

## 3 Results and Discussion

### 3.1 OM Microstructure Analysis

In Fig. 1 the optical microstructure variation of the studied Al–10Si–5Cu alloy before and after strontium addition is shown. Figure 1a, b illustrate the microstructure of the Al–10Si–5Cu alloy without strontium addition. It is commonly known that an Al–10Si–5Cu alloy is mainly composed of

**Table 1** Chemical composition of experimental alloy (wt%)

Si	Cu	Zr	Mg	Mn	Zn	RE	V	Cr	Ni	Al
10	5	0.8	0.75	0.55	0.5	0.3	0.08	0.03	0.025	Bal.

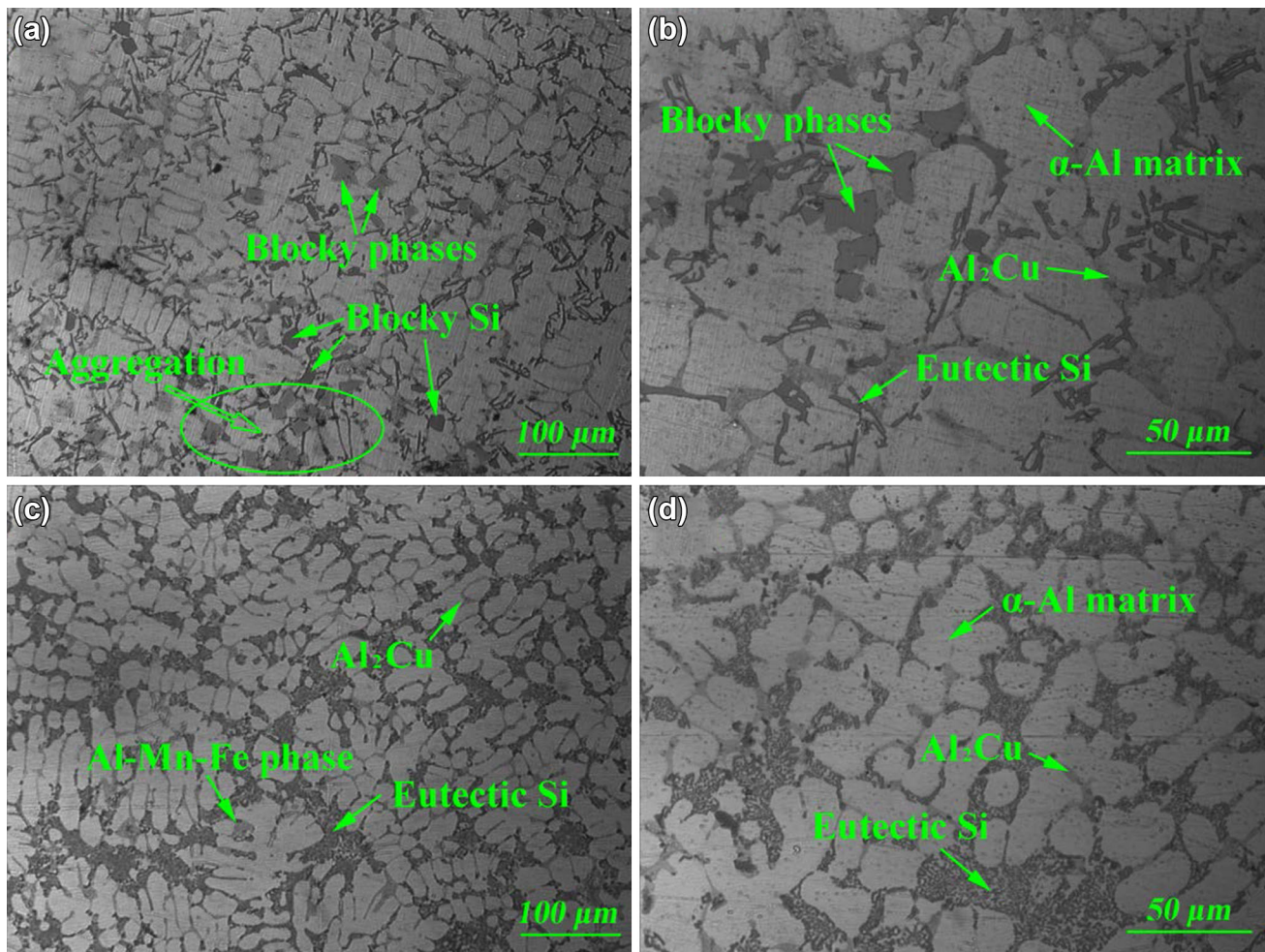


**Fig. 1** Optical micrographs of cast Al-10Si-5Cu alloy, **a, b** before modification, **c, d** after modification

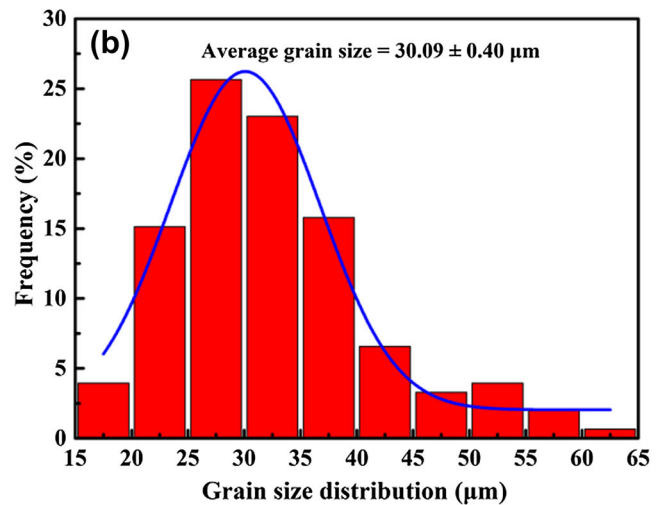
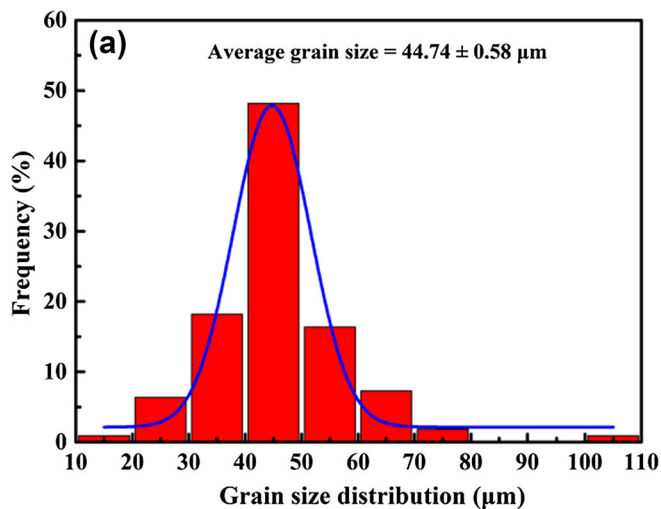
the  $\alpha$ -Al matrix, eutectic Si phase and  $\text{Al}_2\text{Cu}$  phase. In Fig. 1a, it can be observed that eutectic Si and  $\text{Al}_2\text{Cu}$  phases are located at the boundaries of  $\alpha$ -Al grains. Also, a small amount of expected blocky Si phases (with dark color), together with a few star-like blocky phases which tend to aggregate can also be observed. The eutectic Si phase is an acicular lamellar phase with dark color, and the  $\text{Al}_2\text{Cu}$  phase is presented with a lighter color, as shown in Fig. 1b. Nevertheless, in the Al-10Si-5Cu alloy with strontium addition, it is easy to locate the areas with the rounding  $\alpha$ -Al grains, as shown in Fig. 1c. The acicular and lamellar eutectic Si is transformed into a fine fibrous configuration. In addition, the blocky Si phases and star-like blocky phases that are shown in Fig. 1b are not easy to find in this case. Accordingly, it can be ascertained that the addition of an Al-10Sr master alloy will alter the shape and size of  $\alpha$ -Al grains and the morphology of interdendritic phases. In combination with the microstructure variation, the size decrease of  $\alpha$ -Al grains in Al-10Si-5Cu alloy with strontium addition is worth to be noted.

Figure 2 shows the statistical chart of grain size distribution in the Al-10Si-5Cu alloy before and after strontium addition. The size of the grain in the un-modified alloy mainly ranges from 30 to 60  $\mu\text{m}$ , as shown in Fig. 2a. In the alloy with strontium addition, the grain size ranges primarily from 20 to 40  $\mu\text{m}$ , as shown in Fig. 2b. Besides, the distribution of grain size is fitted with a Gaussian function, as the blue curve depicts in Fig. 2. The fitting results indicate that the average grain size of un-modified alloy is  $44.74 \pm 0.58 \mu\text{m}$  while the average grain size becomes  $30.09 \pm 0.40 \mu\text{m}$  in size in the alloy with strontium addition. Comparing the grain sizes in both the alloys, it can be observed that strontium addition leads to a decrease in the grain size.

### 3.2 SEM and EDS Analysis of Interdendritic Phases

In Fig. 3 SEM images of interdendritic phases of Al-10Si-5Cu alloy are shown. In the un-modified Al-Si alloy, the low energy  $\{111\}$  planes are the most





**Fig. 2** Statistics of grain size of alloy, **a** before strontium addition, **b** after strontium addition

thermodynamically stable facets for the nucleation of the Si element, and the Si phase embryo can grow in an unique  $\langle 112 \rangle$  orientation [23, 24]. The specific nucleation and growth of silicon determine an acicular or lamellar eutectic Si phase in the un-modified alloy. In Fig. 3a–c the main interdendritic phases that exist in the Al–10Si–5Cu alloy without strontium are shown. In addition to the commonly known eutectic Si and  $\text{Al}_2\text{Cu}$  phases, a small quantity of blocky Si and  $\text{AlSiMnFe}$  phases have been detected. In Fig. 3c, the EDS spectrum of  $\text{AlSiMnFe}$  phase is shown. Actually, it can be identified that this phase also includes microalloying elements such as V and Ni. It has been reported that the fraction area and size of the  $\text{AlSiMnFe}$  phase can increase in size with the increase of Cr content [25]. Therefore, the obvious aggregation of the  $\text{AlSiMnFe}$  phase in Fig. 1a may be related to the addition of Cr, V and Ni trace elements.

Furthermore, a grain refining efficiency has also been identified in interdendritic phases (including eutectic Si,  $\text{Al}_2\text{Cu}$  phases and  $\text{AlSiMnFe}$  phase) of the alloy with strontium addition. As the  $\text{AlSiMnFe}$  phases became refined, it becomes harder to be distinguished in the OM pictures (Fig. 1c, d). Due to the low solubility of strontium in aluminum, the strontium element is continuously rejected by the solid–liquid interface. Probably, the rejected strontium atoms have some effect in the refining of  $\alpha$ -Al grains and the  $\text{AlSiMnFe}$  phases (shown in Fig. 1c, d). It is identified, that the concentrated strontium atoms surround the  $\alpha$ -Al grains and the  $\text{AlSiMnFe}$  phases to inhibit growth [21, 22]. Also, an undercooling can occur in front of the solid–liquid interface due to the gathering of strontium atoms. This can result in the refinement of the  $\alpha$ -Al grains and the  $\text{AlSiMnFe}$  phases. Moreover, the rejected strontium atoms have an impact on the configuration of the eutectic Si phase. There have been

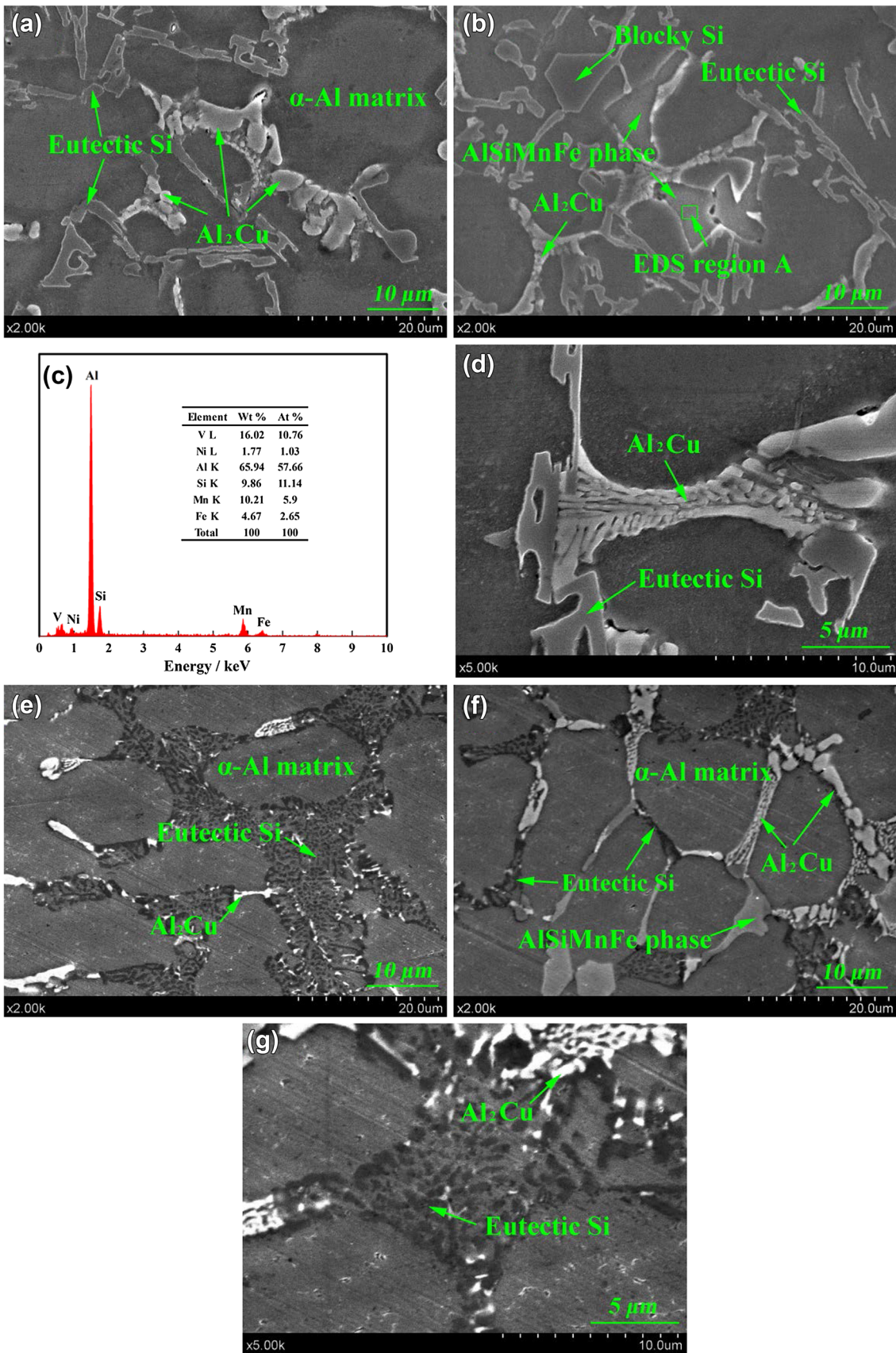
**Fig. 3** SEM and EDS analysis of interdendritic phases before and after strontium addition, **a–d** before addition, **e–g** after addition

numerous studies on the formation mechanisms of eutectic Si phases modified by strontium, which shows that the impurity-induced twinning mechanism (IIT) is the most widely accepted one [26].

### 3.3 XRD Analysis

In Fig. 4 the X-ray diffraction patterns of as-cast Al–Si–Cu alloys before and after strontium modification are shown. In both samples, the  $\alpha$ -Al matrix, the Si phase, the  $\text{Al}_2\text{Cu}$  phase and the  $\text{Al}_{0.93}\text{Cu}_{1.07}$  Mg were detected. In Fig. 4a, the peaks of the alloy without strontium addition appear at  $2\theta$  equal to  $38.322^\circ$ ,  $44.581^\circ$ ,  $64.963^\circ$  and  $78.122^\circ$  and correspond to the (111), (200), (220) and (311) planes of the  $\alpha$ -Al, respectively. Compared to the peaks position of pure aluminum, a slight left shift of Al peaks were identified in Fig. 4a, implying that micro-addition of alloying elements dissolved in the alloy in a limited way was identified and consequently increased the spacing of crystal planes. In addition, as shown in Fig. 4b, the  $2\theta$  of (111), (200), (220) and (311) peaks changed to  $38.442^\circ$ ,  $44.662^\circ$ ,  $65.08^\circ$ ,  $78.223^\circ$  after strontium addition, respectively.

Comparing the diffraction patterns of before and after strontium addition, it is observed that the strongest peak of un-modified alloy is the (200) peak. However, in the strontium modified alloy, the peak changes to become the (111) peak. According to the Al–Si binary phase diagram, the Si phase pre nucleates in the process of solidification. It is known that the growth of eutectic Si phases will be restricted to the  $\langle 112 \rangle$  orientation of the {111} faces due to a more thermo dynamical stability [23]. Despite the





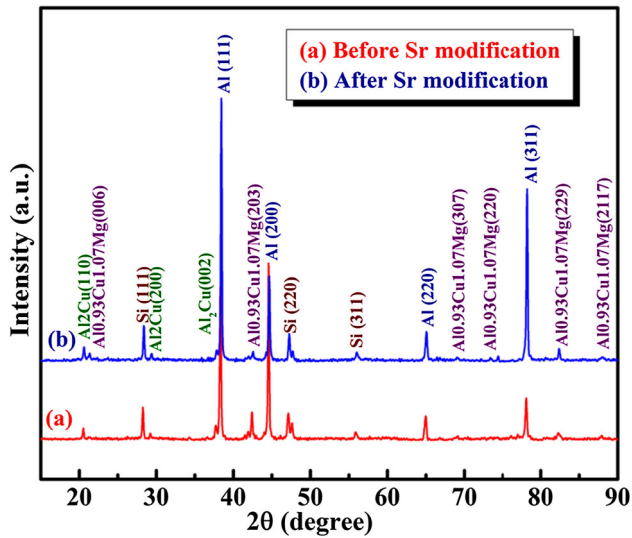


**Fig. 4** XRD profiles of the Al–10Si–5Cu before and after Sr addition

$\langle 112 \rangle$  orientation, the  $\langle 100 \rangle$  and the  $\langle 110 \rangle$  orientations are the optional directions for the growing and the branching eutectic Si phases [24]. For a crystal to grow in the (111) plane along the  $\langle 100 \rangle$  orientation, it means that a final plane will be the (111) one. In addition, it is well known that the  $\alpha$ -Al can nucleate and grow along with the eutectic Si phase. Hence, it can be interpreted that strontium modification increases the number of the (111) planes and enhances the intensity of the (111) peak in the diffraction pattern.

### 3.4 Mechanical Properties

The values of tensile strength, elongation and microhardness are  $305 \pm 5$  MPa,  $2.5 \pm 0.2\%$  and  $144 \pm 4$  HV in samples without modification, respectively. Nevertheless, the alloy without Sr addition may not be a good candidate for application because of the elongation (2.5%).

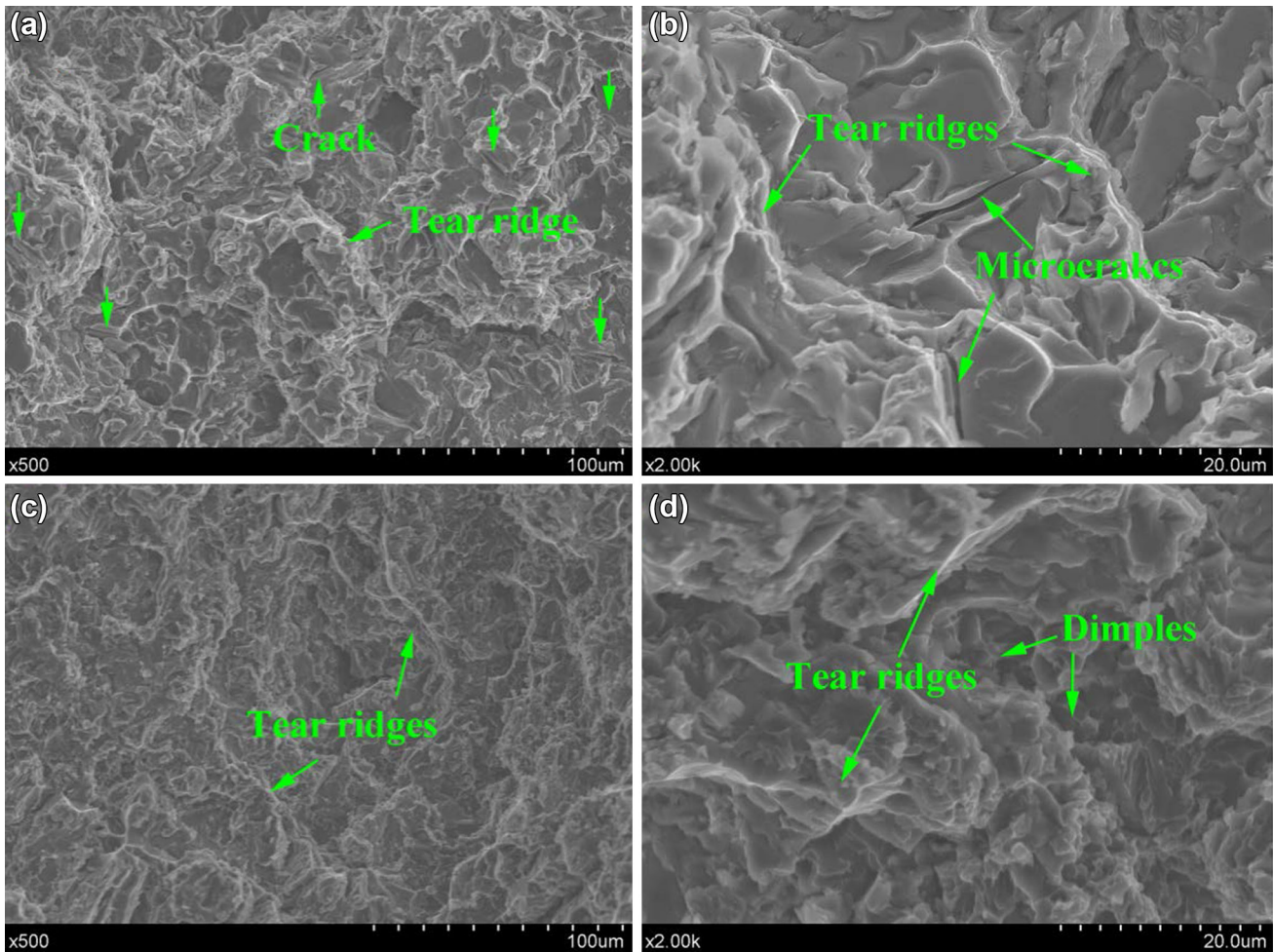


**Fig. 5** SEM images of fracture surfaces of the Al–10Si–5Cu alloy before and after strontium addition, **a, b** before addition, **c, d** after addition

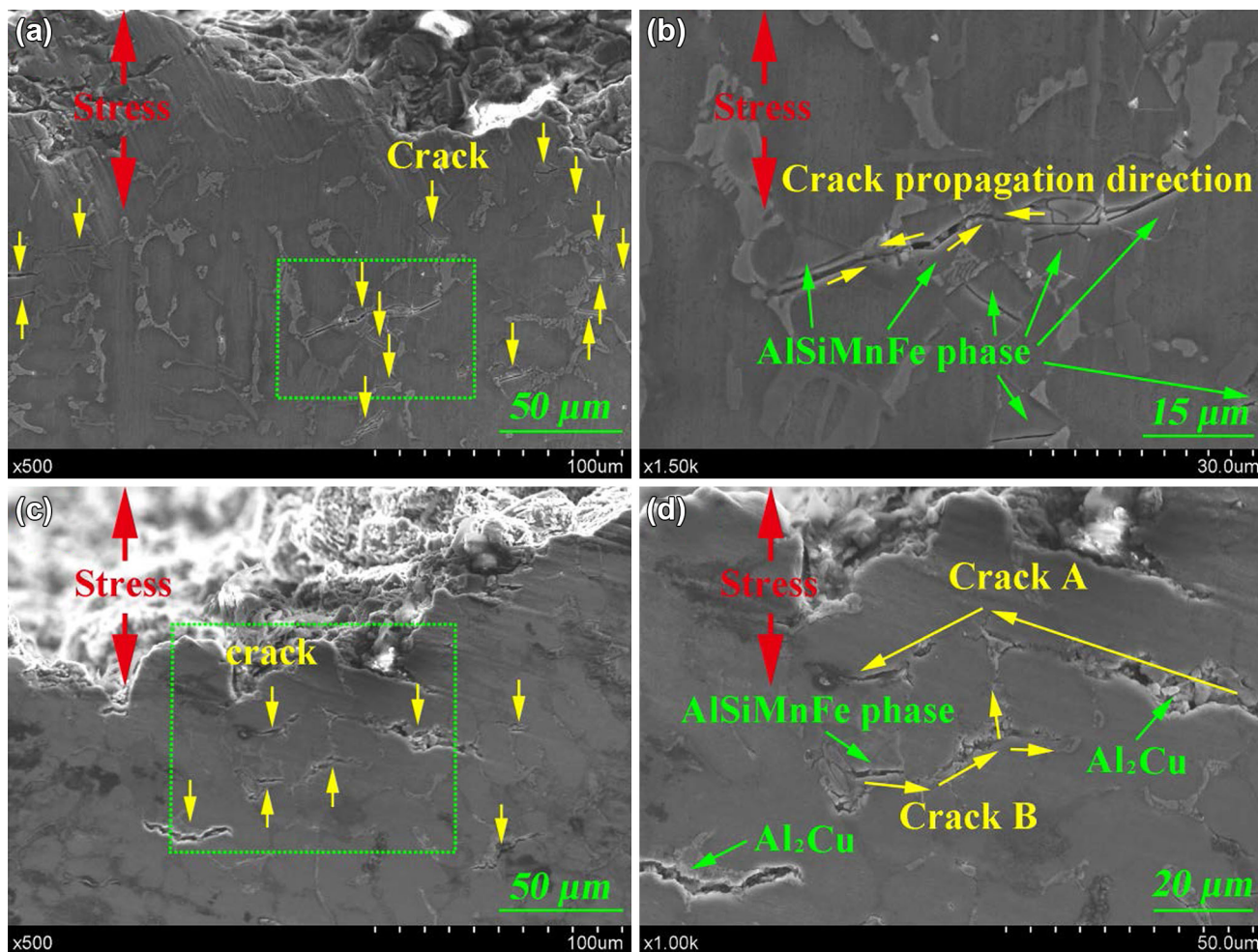


**Fig. 6** SEM images of the cross sections of the Al–10Si–5Cu alloys before and after strontium addition, **a, b** before addition, **c, d** after addition

Hence, Sr is added to improve the plasticity of the alloy. In case of the strontium added alloy, the tensile strength and elongation increases to  $316 \pm 5$  MPa and  $3.4 \pm 0.2\%$ , respectively. Nevertheless, the micro-hardness decreases to  $125 \pm 5$  HV. Owing to the effects of grain refining and interdendritic phase modification, the elongation of the Al–10Si–5Cu alloy is enhanced. Moreover, the effects of grain refining also facilitate the improvement of tensile strength. Regarding the reduced micro-hardness in the strontium modified Al–10Si–5Cu alloy, a reasonable explanation can be that the fine interdendritic phases provide a smaller resistance to the indenter compared to the interdendritic phases in the un-modified alloy, as shown in Fig. 3.

### 3.5 Fracture Surface and Cross Section Morphology

In Fig. 5, the SEM images of the tensile fracture surface of as-cast Al–10Si–5Cu before and after strontium addition are shown. In Fig. 5a, the fractography of the alloy without modification is illustrated. Obvious cleavage planes can be

observed, implying a brittle nature of the alloy in this case. Moreover, cracks are easy to find in the cleavage planes or along with the tear ridges, as shown in Fig. 5b. In Fig. 5c, d the fractography of the alloy with strontium addition is illustrated. It can also be observed that a number of dimples are distributed between the tear ridges. Besides, no obvious cracks are observed in this case. The presence of dimples indicates that strontium addition improves the ductility of the alloy.

For insight provision into the fracture mechanism of Al–10Si–5Cu alloys before and after strontium addition, cross section studies are conducted on the tensile test sample. In Fig. 6, the cross section microstructure of samples after tensile test is shown. In the sample without strontium addition, cracks mainly appear in the blocky fragile AlSiMnFe phases, as shown in Fig. 6a. In Fig. 6b, the details of the cracks in Fig. 6a, are presented. From Fig. 6b, it can be observed that cracks are initiated in the AlSiMnFe phase when a load is being applied. As the applied stress continues, the cracks penetrate through the



matrix in the direction of the yellow arrows. In the strontium alloyed sample, the cracks are primarily present in the interdendritic regions, as shown in Fig. 6c. The region in Fig. 6c that is marked with a green rectangle, is magnified in Fig. 6d. It has been discovered that the cracks mainly initiate from interdendritic phases such as the AlSiMnFe phase or the Al<sub>2</sub>Cu phase. And then the cracks propagate along the grain boundaries.

A large number of blocky AlSiMnFe phases which exist as cracks, function as crack sources in the alloy without strontium addition. Therefore, the location where the AlSiMnFe phases exist as aggregates (shown in Fig. 1a) can form a big crack and tear apart the tensile sample quickly. However, inside the alloy with strontium addition, the blocky AlSiMnFe phases transform into small sized precipitates. This means that, fewer number of cracks can nucleate in this case. Furthermore, the transmission of these initiatory cracks can be restrained by the softer matrix. As a consequence, the cracks can propagate through the relatively brittle grain boundary. Based on the analysis of cracks initiation and propagation, it is easy to understand the enhanced strength and elongation of the alloy with strontium addition.

#### 4 Conclusions

The microstructure and mechanical properties of Al–10Si–5Cu before and after strontium addition were studied. Based on the present findings, the conclusions are:

1. The microstructure of studied Al–10Si–5Cu alloy mainly composed of the  $\alpha$ -Al matrix, the Al<sub>2</sub>Cu phase and the eutectic Si. The strontium addition resulted in the refinement of the  $\alpha$ -Al grains and the interdendritic phases (especially of the blocky AlSiMnFe phases).
2. The Al–10Si–5Cu alloy without strontium addition indicated a brittle nature as a property. Cracks were easily initiated in the fragile AlSiMnFe phases. The propagation of cracks could lead to an abrupt fracture of the alloy.
3. In the strontium alloyed Al–10Si–5Cu samples, cracks initiated mainly at the grain boundaries and propagated along the grain boundaries.
4. On the basis of different crack initiation and propagation behaviors in the Al–10Si–5Cu alloy before and after strontium addition, the strontium addition had

effects in the resistance enhancement of the Al–10Si–5Cu alloy to crack initiation. Therefore, the alloy with strontium addition displayed a better mechanical property than the Al–10Si–5Cu alloy without its addition.

**Acknowledgements** This work was supported by the Natural Science Foundation of Jiangsu province, China under Grant No. BK2011524.

#### References

1. Li Q, Xia T, Lan Y, Zhao W, Fan L, and Li P, *J Alloy Compd* **562** (2013) 25.
2. Vijeesh V, and Prabhu K N, *Trans Ind Inst Met* **67** (2014) 1.
3. Liu G L, Si N C, Sun S C, and Wu Q F, *T Nonferr Metal Soc* **24** (2014) 946.
4. Chang S Y, Tsao L C, Lei Y A, Mao S M, and Huang C H, *J Mater Process Tech* **212** (2012) 8.
5. Fan K L, He G Q, Liu X S, Liu B, She M, Yuan Y L, Yang Y, and Lu Q, *Mater Sci Eng A* **586** (2013) 78.
6. Délia F, and Ravindran C, *Trans Ind Inst Met* **62** (2009) 315.
7. Wang Y, Liao H, Wu Y, and Yang J, *Mater Des* **53** (2014) 634.
8. Kumar V, and Bichler L, *Trans Ind Inst Met* **68** (2015) 1173.
9. Hekmat-Ardakan A, Liu X, Ajersch F, and Chen X G, *Wear* **269** (2010) 684.
10. Banerjee S, Robi P S, Srinivasan A, and Lakavath P K, *Mater Des* **31** (2010) 4007.
11. Shaha S K, Czerwinski F, Kasprzak W, Friedman J, and Chen D L, *Int J Fatigue* **70** (2015) 383.
12. Seifeddine S, Johansson S, and Svensson I L, *Mater Sci Eng A* **490** (2008) 385.
13. Yu S, Jin Y, Xiong W, and Liu Y, *J Rare Earth* **31** (2013) 198.
14. McCartney D G, *Int Mater Rev* **34** (1989) 247.
15. Murty B S, Kori S A, and Chakraborty M, *Int Mater Rev* **47** (2002) 3.
16. Wang T, Chen Z, Fu H, Xu J, Fu Y, and Li T, *Scr Mater* **4** (2011) 1121.
17. Zhao H, Song Y, Li M, and Guan S, *J Alloy Compd* **508** (2010) 206.
18. Li P, Liu S, Zhang L, and Liu X, *Mater Des* **47** (2013) 522.
19. Lu L, Nogita K, and Dahle A K, *Mater Sci Eng A* **399** (2005) 244.
20. Nogita K, Yasuda H, Yoshiya M, McDonald S D, Uesugi K, Takeuchi A, and Suzuki Y, *J Alloy Compd* **489** (2010) 415.
21. Li J H, Zarif M Z, Albu M, McKay B J, Hofer F, and Schumacher P, *Acta Mater* **72** (2014) 80.
22. Li J H, Wang X D, Ludwig T H, Tsunekawa Y, Arnberg L, Jiang J Z, and Schumacher P, *Acta Mater* **84** (2015) 153.
23. Makhlof M, *Int J Metalcast* **4** (2010) 47.
24. Zu F Q, and Li X Y, *China Foundry* **11** (2014) 287.
25. Timelli G, and Bonollo F, *Mater Sci Eng A* **528** (2010) 273.
26. Timpel M, Wanderka N, Schlesiger R, Yamamoto T, Lazarev N, Isheim D, Schmitz G, Matsumura S, and Banhart J, *Acta Mater*, **60** (2012) 3920.